Full paper

Applied Organometallic Chemistry

Received: 2 April 2016 Revised: 21 April 2016 Accepted: 7 May 2016 Published online in Wiley Online Library

(wileyonlinelibrary.com) DOI 10.1002/aoc.3530

A green biosynthesis of NiO nanoparticles using aqueous extract of *Tamarix serotina* and their characterization and application

M. A. Nasseri*, F. Ahrari and B. Zakerinasab

Nickel oxide nanoparticles were prepared using nickel nitrate as precursor with extract of *Tamarix serotina* flowers and were characterized using powder X-ray diffraction, infrared and UV spectroscopies, transmission electron microscopy, vibrating sample magnetometry and BET surface area measurements. Also, the nickel oxide nanoparticles were used as a green and recyclable nanocatalyst for the synthesis of quinoline derivatives. The products are obtained in good to high yields (60–90%) from a one-pot reaction of 2-aminobenzophenone and various carbonyl compounds. Copyright © 2016 John Wiley & Sons, Ltd.

Keywords: nanoparticle; *tamarix serotina*; nano-NiO; green chemistry

Introduction

In recent years, among various nanomaterials, nickel oxide nanoparticles have attracted increasing attention because of their use in a variety of applications such as catalysis,[1] battery cathodes,[2,3] gas sensors,[4] electrochromic films[5] and magnetic materials.[6,7] They are also extensively used in dye-sensitized photocathodes.[8] Also, because of the volume effect, the quantum size effect, the surface effect and the macroscopic quantum tunnel effect, nanocrystalline NiO is expected to possess many improved properties compared to micrometre-sized NiO particles. Therefore, nickel oxide nanoparticles have attracted much attention as an inexpensive and non-hazardous catalyst or an effective promoter that can enhance the reactivity and selectivity of various organic reactions.[9,10]

On a different note, the syntheses of quinolines have been of considerable interest to chemists because their oxygen heterocycles may contribute to potential anti-malarial, anti-bacterial, anti-asthmatic, anti-hypertensive, anti-inflammatory, anti-platelet and tyro kinase PDGF-RTK inhibiting properties.[11–17] For the synthesis of quinolines, various methods have been reported including the Skraup,[18] Conrad–Limpach–Knorr,[19,20] Pfitzinger,[21,22] Friedländer[23,24] and Combes[25,26] methods. However, the Friedländer condensation is still considered as a popular method for the synthesis of quinoline derivatives.[27–31] In this method, 2-aminobenzophenone condenses with ketones or β-diketones to yield quinolines. Nevertheless, the development of new synthetic methods for the efficient preparation of heterocycles containing quinoline fragments is therefore an interesting challenge.

In continuation of our work on the synthesis of efficient and nontoxic nanocatalysts and their application in syntheses of biologically important compounds,[32–38] in the work reported here, we synthesized nickel oxide nanoparticles using aqueous extract of *Tamarix serotina* and evaluated their catalytic activity in the preparation of quinoline derivatives. Quinolines were produced in good to high yields (60–90%) by treatment of 2-aminobenzophenone with various carbonyl compounds (Scheme 1).

Results and discussion

Synthesis and characterization of nickel oxide nanoparticle catalyst

Due to the reasonable needs for clean and green recovery of the heterogeneous catalyst, we synthesized nickel oxide nanoparticles using aqueous extract of *T. serotina*. The aqueous extract was prepared using dried flowers in deionized water as precursor. For the formation of nickel oxide nanoparticles, nickel nitrate hexahydrate in deionized water was reacted with aqueous extract of *T. serotina* by heating at 115 °C for 1.5 h in an oil bath. The resulting compound was dried and was calcined at 400 °C for 1 h (Scheme 2). Various approaches such as transmission electron microscopy (TEM), infrared (IR) and UV spectroscopies, vibrating sample magnetometry (VSM), powder X-ray diffraction (XRD) and BET surface area measurements were used to characterize the precursors and NiO nanoparticles.

TEM analysis of NiO nanoparticles

TEM analysis of the products (Fig. 1) provides information on the size and morphology of the NiO nanoparticles and their status of agglomeration. The results show the average product size of NiO nanoparticles as 10 and 14 nm (Fig. 2) similar to the results from XRD patterns. The uniform NiO particles have spherical shapes with weak agglomeration. According to the TEM image, it can be concluded that this preparation method for the precursor obtained by homogeneous precipitation had successfully overcome the problem of agglomeration and the calcination condition

* *Correspondence to: M. A. Nasseri, Department of Chemistry, College of Sciences, University of Birjand, Birjand 97175-615, Iran. E-mail: manaseri@birjand.ac.ir*

Department of Chemistry, College of Sciences, University of Birjand, Birjand 97175-615, Iran

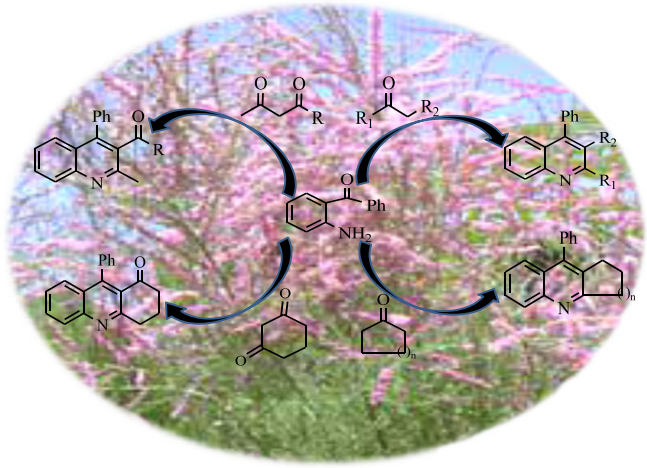

Scheme 1. Green synthesis of quinolines catalysed by nickel oxide nanoparticles.

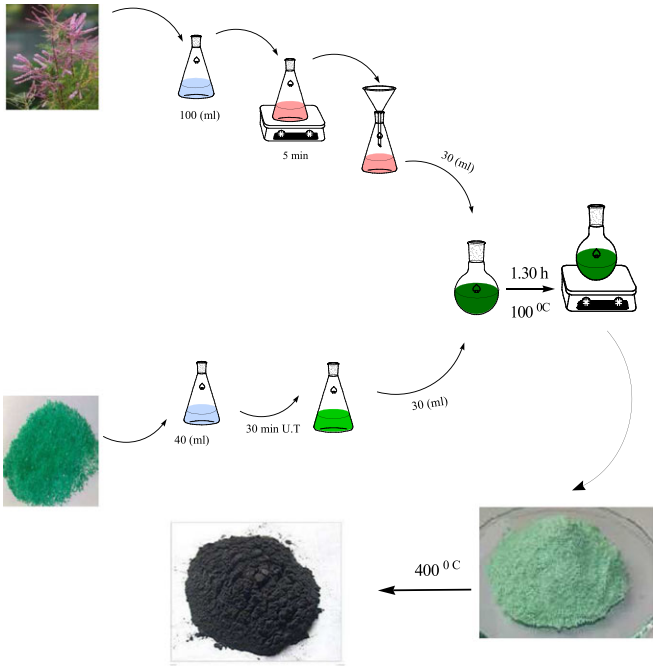

Scheme 2. Biosynthesis of nickel oxide nanoparticles.

(400 °C for 1 h) was appropriate for obtaining the NiO nanoparticles of small crystalline size.

XRD analysis of NiO nanoparticles

The XRD pattern of NiO nanoparticles was obtained. As shown in Fig. 3, the XRD pattern of NiO nanoparticles indicates a crystallized structure with peaks at $2\theta = 37.10°$, 43.30°, 62.88°, 75.55° and 79.30° and their lattice parameters are quite consistent with those of JCPDS card no. 04–0835 for the standard spectrum of pure NiO. The results indicate that the products were nano-NiO crystals of cubic structure; they have a high purity and small particle size with a fine crystal phase. The size of these particles could be estimated using the Debye–Scherrer equation ($D = 0.89\lambda/\beta \cos\theta$, where D is the average particle size, β is the full width at half-height of the peaks, λ is the X-ray wavelength and θ is the diffraction angle of the peak), from which the mean particle size of the as-synthesized products is calculated at about 5.29–8.31 nm.

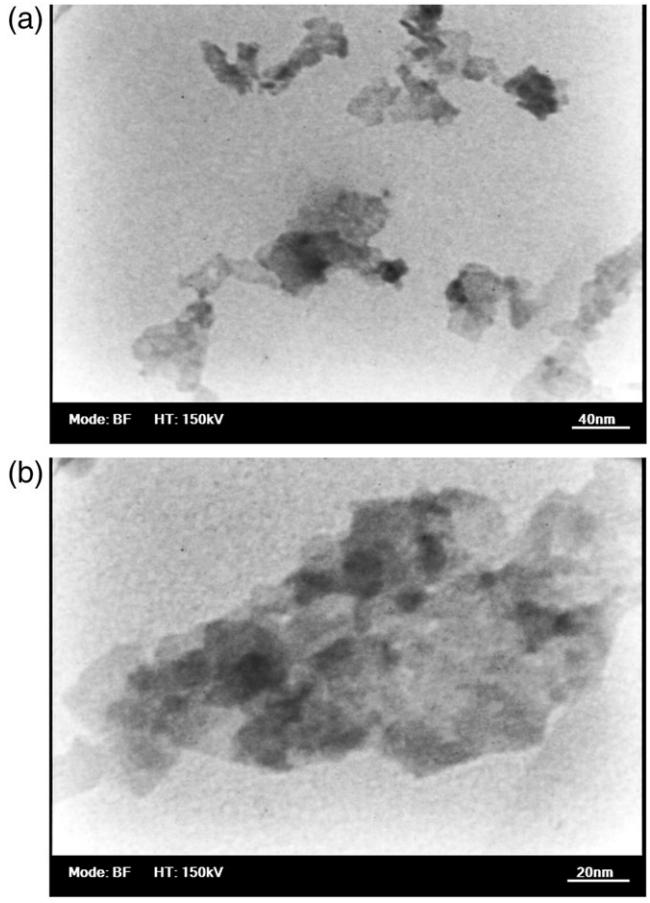

Figure 1. TEM images of (a) NiO nanoparticles and (b) NiO nanoparticles reused after five runs.

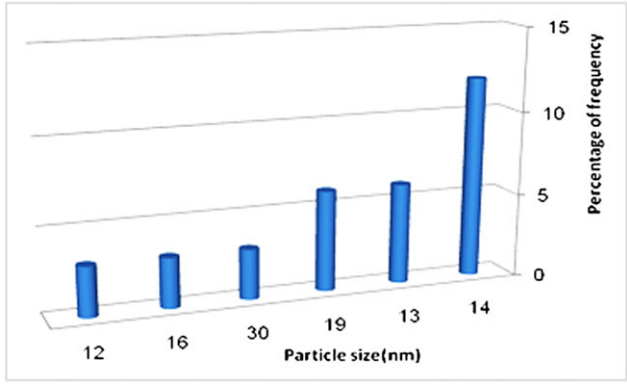

Figure 2. Particle size distribution of NiO nanoparticles.

IR spectral analysis of NiO nanoparticles

The IR spectra from 4000 to 600 cm^{-1} for $Ni(OH)_2$ and NiO powders as a function of heat treatment temperature were obtained, and the results are shown in Fig. 4. The broad absorption peak at 3450 cm^{-1} belongs to OH stretching vibrations. The peak located at 1628 cm^{-1} is attributed to the bending mode (H–O–H) of water molecules. According to the IR spectrum of $Ni(OH)_2$, the vibration bands at 2395, 1762 and 812 cm^{-1} are due to $NaNO_3$ as a by-product of the reaction. The intense and sharp band at 1430 cm^{-1} is characteristic of interlayer NO_3^-. The small band at about 698 cm^{-1} is ascribed to the Ni–O–H vibration. The absence

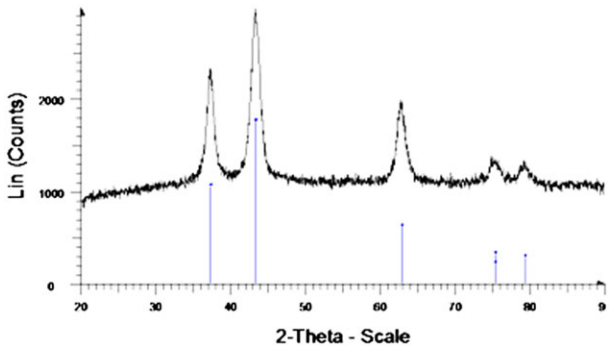

Figure 3. XRD pattern of NiO nanoparticles.

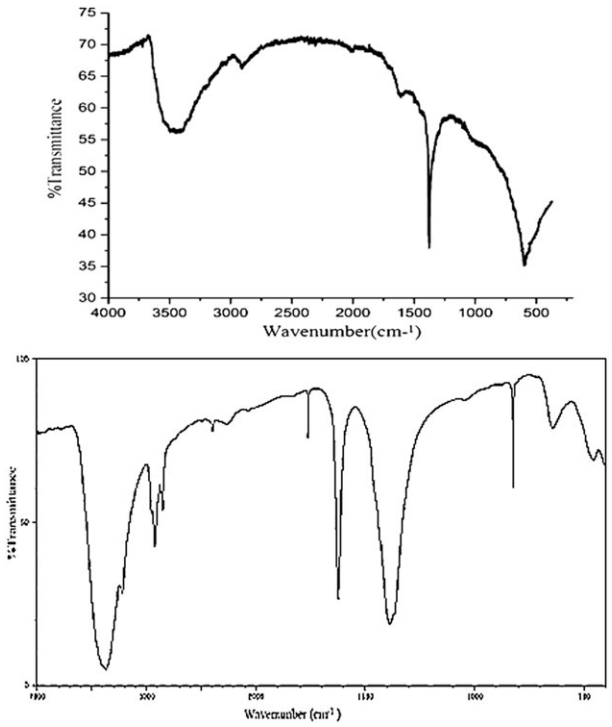

Figure 4. IR spectra of $Ni(OH)_2$ (bottom) and NiO nanoparticles (top).

of a band at 698 cm^{-1} in the spectrum of NiO indicates the loss of hydroxyl group of $Ni(OH)_2$. The obtained peak at 510 cm^{-1} is caused by the Ni–O vibration.

UV spectral analysis of NiO nanoparticles

UV–visible spectra of $NiNO_3$, $Ni(OH)_2$ and NiO nanoparticles are shown in Fig. 5. In to the UV spectrum of $NiNO_3$, the absorption peak at 350–450 nm is due to water in the structure of $NiNO_3{\cdot}6H_2O$. This absorption peak is absent in the UV–visible spectra of $Ni(OH)_2$ and NiO. A strong absorption peak at 296 nm is observed, attributable to the n to π^* transition of Ni–O bonds.

BET analysis of NiO nanoparticles

The BET surface area and the pore size distribution of the calcined nanopowders were determined with a BET surface area analyser using nitrogen as the adsorptive gas. The specific surface area of the nano-NiO products calculated using the BET method is

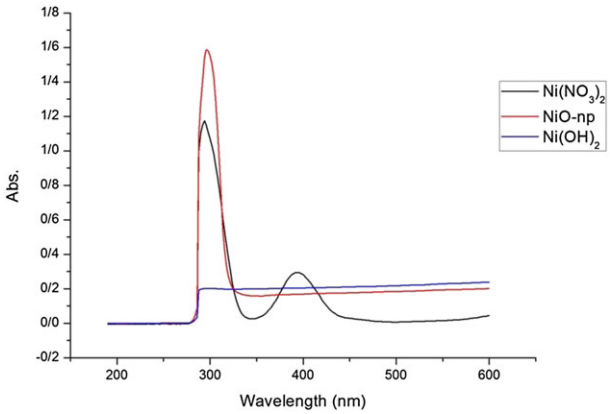

Figure 5. UV–visible spectra of $NiNO_3$, $Ni(OH)_2$ and NiO nanoparticles.

126.16 $m^2\ g^{-1}$. The much higher external surface area of the NiO nanoparticles is most likely attributed to their smaller particle size. The BET specific surface areas were obtained from the isotherms (Fig. 6) for the specimens and the resulting pore size distribution curves are shown in Fig. 7. According to the results, the pore size of nano-NiO products calculated from the BJH curve is 13 nm which

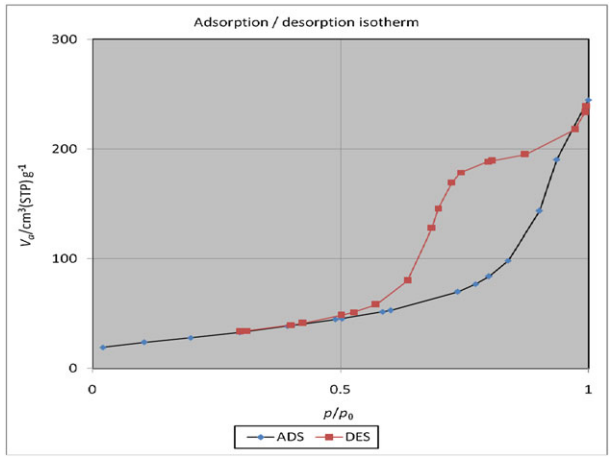

Figure 6. BET isotherm of NiO nanoparticles.

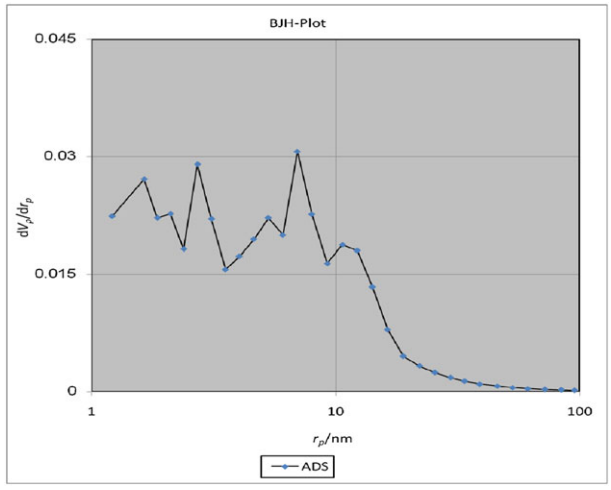

Figure 7. BJH spectrum of NiO nanoparticles.

is obtained by substituting the XRD results in the Debye–Scherrer formula.

VSM analysis of NiO nanoparticles

The magnetic properties of the sample containing a magnetite component were studied using VSM at 300 K (Fig. 8). Figure 8 shows the absence of hysteresis phenomenon and indicates that the product has superparamagnetism at room temperature. The saturation magnetization for nano-NiO particles is 353 emu g^{-1}.

Evaluation of catalytic activity of NiO nanoparticles for synthesis of quinolines

As we know, the much higher external surface areas of the nano-NiO products indicate the possibility of their application as an efficient catalytic material. In order to show the merit of the synthesized nanocatalyst in organic reactions, the NiO nanoparticles were used for the synthesis of quinolines by treatment of 2-aminobenzophenone and carbonyl compounds. In order to evaluate the catalytic efficiency of the NiO nanoparticles and to determine the most appropriate reaction conditions; initially a model study was carried out of the synthesis of quinoline by the condensation of 2-aminobenzophenone and acetylacetone under a variety of reaction conditions. In a preliminary experiment, this reaction was carried out in various solvents, with NiO nanoparticles (0.004 g) as a catalyst. The reaction can be carried out in various solvents and gives product in low yield (Fig. 9). It is very surprising that the reaction proceeds in excellent yields (86%) in ethylene glycol as solvent. To determine the effect of the amount of solvent on the synthesis of quinoline, we changed the amount of ethylene glycol.

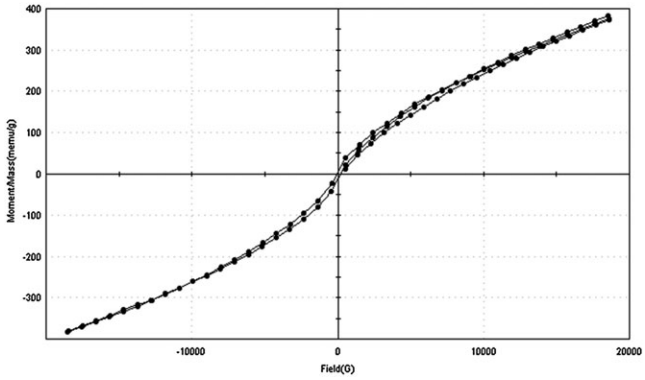

Figure 8. VSM pattern of NiO nanoparticles.

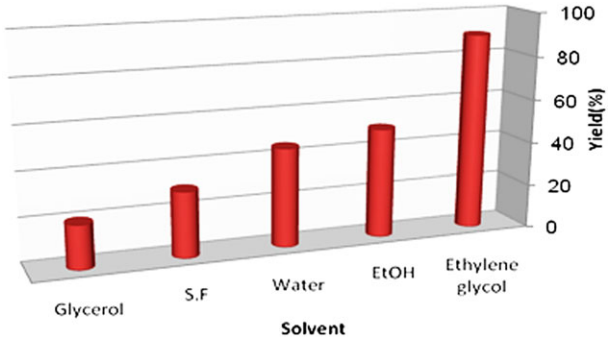

Figure 9. Effect of solvent on synthesis of quinoline.

The results are summarized in Fig. 10 showing that 0.1 ml of ethylene glycol is the optimum amount of solvent.

To further optimize the reaction conditions, we also changed the temperature and the amount of catalyst. The results are summarized in Figs 11 and 12. The reaction proceeds perfectly at high temperature, but the yields decrease when the reaction is carried out at low temperature. Consequently, among the tested temperature and the amount of catalyst, the condensation of 2-aminobenzophenone and acetylacetone is best catalysed by 0.004 g of NiO nanoparticles at 100 °C in 0.1 ml of ethylene glycol as solvent.

To evaluate catalytic activity of the NiO nanoparticles, the model reaction was carried out in ethylene glycol at 100 °C for 2.5 h in the presence of each of various catalytic systems (0.004 g). The results are shown in Fig. 13. As is evident from the results, NiO nanoparticles are the most effective catalyst in terms of yield of quinolines

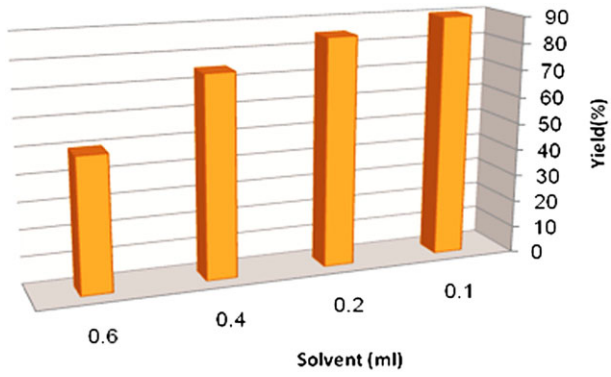

Figure 10. Effect of amount of solvent on synthesis of quinolines.

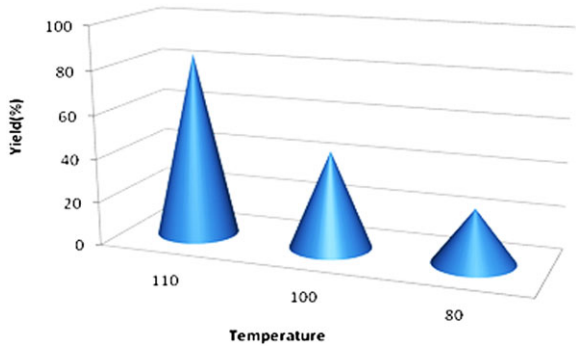

Figure 11. Effect of temperature on synthesis of quinolines.

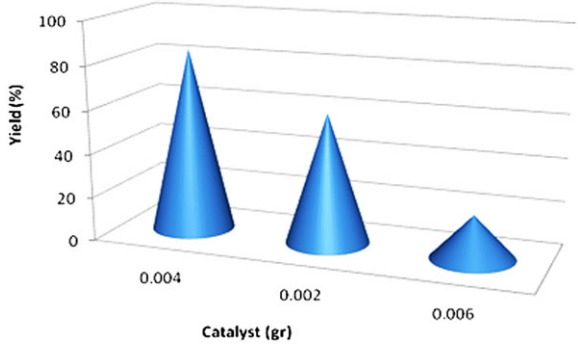

Figure 12. Effect of amount of catalyst on synthesis of quinolines.

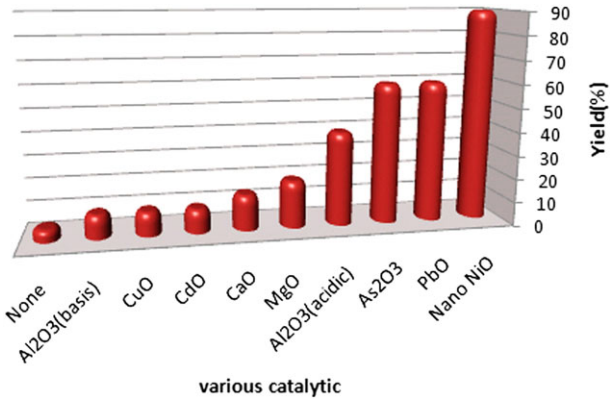

Figure 13. One-pot synthesis of quinoline in the presence of various catalytic systems.

(90%) while the other catalysts lead to product in yields of 5–60%. Control experiments indicate that in the absence of the catalyst, the reaction under the same condition gives quinoline in a rather low yield of 5%.

To establish the generality and applicability of this method, 2-amino-5-chlorobenzophenone/2-aminobenzophenone and carbonyl compounds were subjected to the same reaction conditions to furnish the corresponding quinolines (Table 1). Not only diketones (Table 1, entries 1–4) but also ketones (Table 1, entries 5–10) afford the desired products in good to excellent yields (60–90%) in short reaction time (1–3.5 h). Also, the reaction time of 2-amino-5-chlorobenzophenone and dicarbonyl compounds is longer than that of 2-aminobenzophenone. The reaction of cyclic diketones takes place faster than that of open-chain analogues. These reactions also proceed with ketone derivatives (Table 1, entries 5–8 and 12). In these cases the reaction times are longer. This may be due to the less activity of ketone derivatives than dicarbonyl compounds.

In Table 2, the efficiency of our method for the synthesis of quinolines is compared with some other published works. Each of these methods have their own advantages, but they often suffer from some troubles including the use of organic solvent, long reaction time (entries 3–9) and employ of non-recyclable catalyst (entries 6, 7 and 10).

At the end of the reaction, the catalyst could be recovered by centrifugation. The recycled catalyst was washed with dichloromethane and subjected to another reaction process. The results show that the yield of product after four runs is only slightly reduced (Fig. 14).

A reasonable pathway for the reaction of 2-aminobenzophenone with carbonyl compounds conducted in the presence of nano-NiO is presented in Scheme 3. The first step involves the formation of activated benzophenone by nano-NiO followed by its reaction with carbonyl compound that subsequently undergoes elimination reaction to produce the compound intermediate. The intermediate undergoes further elimination reaction to afford the heterocycle of quinoline.

Experimental

General methods

Quinoline derivatives were purchased from Merck Chemical Company. Purity determination of the products was accomplished using TLC with silica gel Polygram SILG/UV 254 plates. Melting points were measured with an Electro Thermal 9100 apparatus. IR spectra were obtained with a PerkinElmer 781 spectrometer in KBr pellets and reported in cm^{-1}. ^1H NMR and ^{13}C NMR spectra were measured with a Bruker DPX-250 Avance instrument at 250 and 62.9 MHz in $CDCl_3$ or DMSO-d_6 with chemical shifts given in ppm relative to tetramethylsilane as internal standard. The morphology of the products was determined using a CMPhilips10 model TEM instrument at an accelerating voltage of 100 kV. Powder XRD was performed using a Bruker D_8-Advance X-ray diffractometer with Cu K_α (λ = 0.154 nm) radiation.

Table 1. Synthesis of quinolines[a]

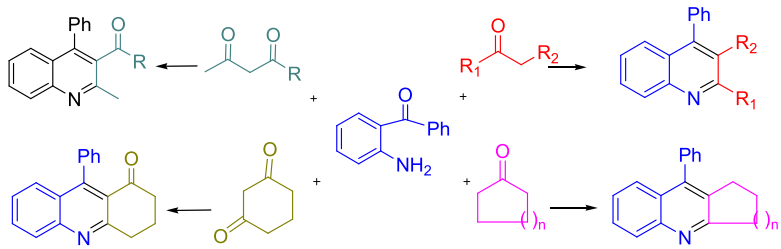

Entry	Substrate 1	Substrate 2	Time (h)	Yield (%)[b]	M.p. (°C)
1	2-Aminobenzophenone	1,3-Cyclohexadione	2	85	155–156[a]
2	5-Chloro-2-aminobenzophenone	1,3-Cyclohexadione	1	90	184[b]
3	2-Aminobenzophenone	Dimedone	3	75	192–194[a]
4	5-Chloro-2-aminobenzophenone	Dimedone	1	80	207–209[a]
5	2-Aminobenzophenone	Cyclohexanone	2	80	153–154[a]
6	5-Chloro-2-aminobenzophenone	Cyclohexanone	3	70	164–166[a]
7	2-Aminobenzophenone	Cyclopentanone	2	80	130–131[a]
8	5-Chloro-2-aminobenzophenone	Cyclopentanone	3	60	106–108[a]
9	2-Aminobenzophenone	Acetylacetone	2.5	90	110–112[a]
10	2-Aminobenzophenone	Methyl acetoacetate	2	80	99–100[a]
11	5-Chloro-2-aminobenzophenone	Ethyl acetoacetate	2	70	269–272[c]
12	2-Aminobenzophenone	4-Chloroacetophenone	3.5	70	103–105[d]

Table 2. Comparison of results using NiO nanoparticles with those obtained by other studies for the synthesis of quinolines

Entry	Catalyst	Condition	Yield (%)[a]	Ref.
1	Current	Ethylene glycol, 100 °C, 2 h	85	—
2	$HClO_4$–SiO_2	CH_3CN, 60 °C, 3 h	92	[35]
3	PMA–SiO_2	EtOH, reflux, 8 h	88	[36]
4	$Zr(DS)_4$	H_2O, reflux, 6 h	90	[37]
5	$Zr(HSO_4)_4$	H_2O, reflux, 13 h	87	[38]
6	CH_3COOH (1 eq.)	H_2O, 60 °C, 6 h	60	[39]
7	*p*-TsOH (1 eq.)	H_2O, 60 °C, 6 h	62	[39]
8	bmimCl–$ZnCl_2$	Ionic liquid, r.t., 24 h	80	[40]
9	H_3PO_4 (1 eq.)	H_2O, 60 °C, 12 h	90	[39]
10	HCl	H_2O, 100–200 °C, 1 h	68	[41]

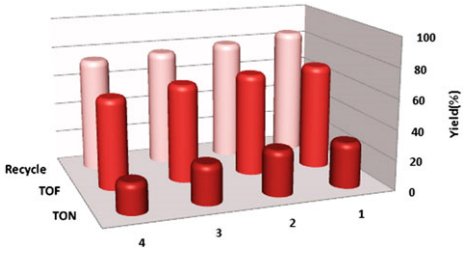

Figure 14. Recycling of catalyst for the synthesis of quinolines.

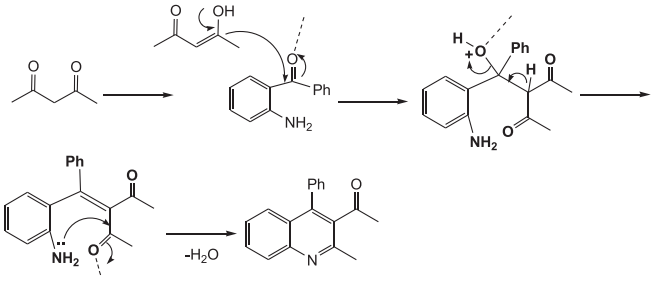

Scheme 3. Proposed mechanism for the synthesis of quinoline in the presence of nano-NiO.

Plant collection and extraction

Tamarix serotina flowers were collected in July 2014 from South Khorasan province, Iran. The AP and R of these plants were separated, washed, shade-dried in air and ground in a mixer. Plant powder (10 g) was added to 100 ml of water and the mixture was stirred for 5 min at boiling temperature and filtered to obtain a clear extract.

Synthesis of NiO nanoparticles

Nickel nitrate hexahydrate (2.63 g) was accurately weighed and dissolved into 40 ml of deionized water and placed under ultrasonic treatment. $Ni(NO_3)_2{\cdot}6H_2O$ solution (30 ml) was mixed with 30 ml of the obtained biological extract and the two solutions were mixed in a beaker and stirred with a magnetic stirrer at room temperature until a homogeneous solution was obtained. Thereafter, the mixture was transferred into a round-bottom flask, sealed and maintained heating at 115 °C for 1.5 h in an oil bath. In this process, a kind of light green sediment was formed. After the reaction was completed, the precipitated powders were filtered and washed with deionized water to neutral to remove the adsorbed ions and chemicals so as to reduce the potential for agglomeration. After being dried in an oven at 90 °C for 6 h, the precursor was calcined in a muffle furnace at 400 °C for 1 h to afford the products with a dark colour (NiO nanoparticles).

General procedure for preparation of quinoline derivatives

To a mixture of carbonyl compounds (1.0 mmol), 2-amino-5-chlorobenzophenone or 2-aminobenzophenone (1.0 mmol) and ethylene glycol (0.1 ml) was added nano-NiO (0.004 g). The mixture was stirred at 100 °C for the appropriate reaction time (Table 1). The progress of the reaction was monitored by TLC. After completion of the reaction, the mixture was dissolved in acetone and the catalyst was isolated by centrifugation. Then the solvent was removed from solution under reduced pressure and the resulting product was purified by recrystallization using ethanol to afford the pure quinoline product in excellent purity and yield. Structural assignments of the products are based on their ^{1}H NMR, ^{13}C NMR, mass and IR spectra.

Acknowledgement

We gratefully acknowledge the support of this work by the Birjand University Research Council.

References

[1] K. M. Dooley, S. Y. Chen, J. R. Ross, *J. Catal.* **1994**, *145*, 402.
[2] H. X. Yang, Q. F. Dong, X. H. Hu, *J. Power Sources* **1999**, *79*, 256.
[3] I. Hotový, J. Huran, L. Spiess, R. Čapkovic, Š. Haščı, *Vacuum* **2000**, *58*, 300.
[4] E. L. Miller, R. E. Rocheleau, *J. Electrochem. Soc.* **1997**, *144*, 3072.
[5] G. Wang, X. Lu, T. Zhai, Y. Ling, H. Wang, Y. Tong, Y. Li, *Nanoscale* **2012**, *4*, 3123.
[6] Y. Ichiyanagi, N. Wakabayashi, J. Yamazaki, S. Yamada, Y. Kimishima, E. Komatsu, H. Tajima, *Physica B* **2003**, *329–333*, 862.
[7] S. A. Makhlouf, F. T. Parker, F. E. Spada, A. E. Berkowitz, *J. Appl. Phys.* **1997**, *84*, 5561.
[8] X. Y. Deng, Z. Chen, *Mater. Lett.* **2004**, *58*, 276.
[9] V. Biju, M. Abdul Khadar, *Mater. Sci. Eng. A* **2001**, *304*, 814.
[10] Y. Wang, J. Zhu, X. Yang, L. Lu, X. Wang, *Thermochim. Acta* **2005**, *437*, 106.
[11] M. P. Maguire, K. R. Sheets, K. McVety, A. P. Spada, A. J. Zilberstein, *Med. Chem.* **1994**, *37*, 2129.
[12] R. D. Larsen, E. G. Corley, A. O. King, J. D. Carrol, P. Davis, T. R. Verhoeven, P. J. Reider, M. Labelle, J. Y. Gauthier, Y. B. Xiang, R. J. Zamboni, *J. Org. Chem.* **1996**, *61*, 3398.
[13] Y. L. Chen, K. C. Fang, J. Y. Sheu, S. L. Hsu, C. C. Tzeng, *J. Med. Chem.* **2001**, *44*, 2374.
[14] G. Roma, M. D. Braccio, G. Grossi, F. Mattioli, M. Ghia, *Eur. J. Med. Chem.* **2000**, *35*, 1021.
[15] B. Kalluraya, S. F. Sreenivasa, *Farmaco* **1998**, *53*, 399.
[16] D. Doube, M. Blouin, C. Brideau, C. Chan, S. Desmarais, D. Eithier, J. P. Fagueyret, R. W. Friesen, M. Girard, Y. Girard, J. Guay, P. Tagari, R. N. Young, *J. Bioorg. Med. Chem. Lett.* **1998**, *8*, 1255.
[17] T. C. Ko, M. J. Hour, J. C. Lien, C. M. Teng, K. H. Lee, S. C. Kuo, L. Huang, *J. Bioorg. Med. Chem. Lett.* **2001**, *11*, 279.
[18] Z. H. Skraup, *Monatsh. Chem.* **1880**, *1*, 316.
[19] N. D. Heindel, T. A. Brodof, J. E. Kogelschatz, *J. Heterocycl. Chem.* **1966**, *3*, 222.
[20] I. Hermecz, G. Kereszturi, L. Vasvari-Debreczy, *Adv. Heterocycl. Chem.* **1992**, *54*, 1.
[21] W. Pfitzinger, *J. Prakt. Chem.* **1886**, *33*, 100.
[22] P. K. Calaway, H. R. Henze, *J. Am. Chem. Soc.* **1939**, *61*, 1355.
[23] P. Friedländer, *Chem. Ber.* **1882**, *15*, 2572.
[24] E. A. Fehnel, *J. Org. Chem.* **1966**, *31*, 2899.
[25] R. Long, K. Schofield, *J. Chem. Soc.* **1953**, 3161.

[26] E. Roberts, E. E. Turner, *J. Chem. Soc.* **1832**, *1927*.
[27] J. S. Yadav, P. Rao, D. Sreenu, R. S. Rao, V. N. Kumar, K. Nagaiah, A. R. Prasad, *Tetrahedron Lett.* **2005**, *46*, 7249.
[28] V. V. Kouznetsov, L. Y. Mendez, C. M. M. Gomez, *Curr. Org. Chem.* **2005**, *9*, 141.
[29] S. J. Song, S. J. Cho, D. K. Park, T. W. Kwan, S. A. Jenekhe, *Tetrahedron Lett.* **2003**, *44*, 255.
[30] S. A. Palimkar, S. A. Siddiqui, T. Daniel, R. J. Lahoti, K. V. Srinivasan, *J. Org. Chem.* **2003**, *68*, 9371.
[31] S. K. De, R. A. Gibbs, *Tetrahedron Lett.* **2005**, *46*, 1647.
[32] M. A. Nasseri, B. Zakerinasab, M. M. Samieadel, *RSC Adv.* **2014**, *4*, 41753.
[33] M. A. Nasseri, F. Kamali, B. Zakerinasab, *RSC Adv.* **2015**, *5*, 26517.
[34] M. A. Nasseri, F. Ahrari, B. Zakerinasab, *RSC Adv.* **2015**, *5*, 13901.
[35] M. A. Nasseri, S. A. Alavi, B. Zakerinasab, *J. Iran. Chem. Soc.* **2013**, *10*, 21.
[36] M. A. Nasseri, M. Salimi, *Lett. Org. Chem.* **2013**, *10*, 164.
[37] M. A. Nasseri, S. M. Sadeghzadeh, *J. Iran. Chem. Soc.* **2014**, *11*, 27.
[38] M. Salimi, M. A. Nasseri, T. Dalliran Chapesshloo, B. Zakerinasab, *RSC Adv.* **2015**, *5*, 33974.
[39] M. Dabiri, S. Bashiribod, *Molecules* **2009**, 14.
[40] M. A. Zolfigol, P. Salehi, M. Shiri, T. Faal Rastegar, A. Ghaderi, *J. Iran. Chem. Soc.* **2008**, *5*, 490.
[41] R. Ghorbani, S. Akbari, *Tetrahedron Lett.* **2009**, *50*, 1055.